Characterisation of carboxylate nanocrystal cellulose /silver nanoparticles from eucalyptus pulp and its antitumour activity

Pasakorn Jutakridsada
Khon Kaen University
Somnuk Theerakulpisut
Khon Kaen University
Mika Sillanpää
King Saud University
Khanita Kamwilaisak (khanita@kku.ac.th)
Khon Kaen University https://orcid.org/0000-0002-5167-4596

Research Article

Keywords: cellulose nanocrystals, nanosilver particles, nanohybrid material, Control releasing, antitumor activity

Posted Date: March 22nd, 2021

DOI: https://doi.org/10.21203/rs.3.rs-331735/v1

Abstract

Cellulose nanocrystal (CNC) has a high prospect in the biomedical field due to its favourable biocompatibility, stability, and modifiable properties, which render it potentially useful as a template for silver deposition nanoparticles (Ag NPs). In this research work, the aim was to prepare AgNPs on carboxylate nanocrystal cellulose (cCNC) in a minimised process and decrease the number of chemical reagents and with a stable anchor and controllable release Ag + by hydrothermal reaction. The controlled release of Ag+ was also determined. The anticancer activity of Ag-cCNC on HCT116 (Human colon cancer cells) and SK-MEL-2 (Human Skin Melanoma cells) were investigated. Silver nanoparticles were uniformly deposited onto cCNC with a 28.0% yield and a particle size of ∼15 nm. The release rate of silver ions was monitored for 32 days by ICOES analysis. It was found that Ag-cCNC induced silver ions to release slowly, which displayed a controllable release of silver ions with a rate of 0.1-0.2% per 2 days and a longterm release of 245 days. Also, Ag-cCNC showed anticancer activity against both HCT 116 (Human colon cancer cell) and SK-MEL-2 (Human Skin Melanoma cell) at 35±4.04% and 20±7.68% cell viability, respectively. Ag-cCNC showed promising higher 15% anticancer HCT 116 efficacy than cisplatin, but it was lower 18% in anticancer SK-MEL-2. This study provides a novel, sustainable, simple and straightforward way with environmentally friendly to produce and use natural composite material from Eucalyptus as an antitumour drug.

Introduction

Over the decade, cancer is a disease group that has caused various pathological and metabolic changes in cellular environments. Cancer is the second most significant cause of death globally. An estimated 9.6 million deaths due to cancer took place in 2018, about 1 in every6 deaths. Mostly, the typical case in 2018 is Lung (22.40%), then Breast (22.40%), Colorectal (19.29%), Prostate (13.72), Skin cancer (11.15%) and Stomach (11.04%) cancers (de Martel et al. 2020). Cancer cells have abnormal metabolic activities in aerobic glycolysis, mitochondrial DNA depletion, alterations in respiratory chains and genomic expressions. The medical therapy of cancer has been used, especially taking chemical medicine (Litwin and Tan 2017). However, some medicine and chemotherapy could be limited by their undesirable side effects to other cells, low solubility, and multidrug resistance (MDR) (Qiao et al. 2010; Somu and Paul 2019). The drug's low solubility has issued a limited bioaccessibility because the insoluble drug had lower diffusion capacity into the human cell membrane, and multidrug resistance is the principal mechanism to involve cancer against chemotherapy drugs. Hence, there is a need for developing an alternate therapeutic approach with selective cytotoxicity to cancer cells with minimal or no toxicity to healthy cells.

Recently, the concept of nanoparticles (NPs) for cancer therapy has been studied. The NPs are investigated in cancer therapy applications as clusters of ions, atoms or molecules within a specified size range of 1–100 nm (Johnston 2012). The NPs such as gold (Au), silver (Ag), and platinum (Pt) nanoparticles size of 70–200 nm were suitable for use in cancer treatment (Gaumet et al. 2008). Silver ions (Ag^+) have been reported as essential components for various antibacterial products because of their antibacterial effect and low-toxicity to human cells (Wu et al. 2018). Moreover, they have been used in the pharmaceutical application of AgNPs by enhancing the tumour-killing effects of anticancer drugs (Chugh et al. 2018). Mostly, AgNPs are unstable because of their large surface, leading to a large cluster in the media. This causes low efficacy activity (Fujii et al. 2020). In general, the prevent aggregation of AgNPs in media has been reported by adding a dispersing agent or surface modification. The addition of extra chemical reagents such as toxic or dispersing reagent is overused to prepare uniform, stable dispersion of AgNPs. The deposition technique of metal nanoparticles with polymer matrices have been used to immobilise Ag NPs, including physisorption, electrostatic binding, and charge-transfer interactions (Harra et al. 2012; Sotiriou 2013; Wu et al. 2018). It has been reported that Ag^+ ions could be released from their support to

inhibit bacterial growth at human body temperature (Ghasemzadeh et al. 2016). However, the drawback of AgNPs on the additive substrate was an uncontrollable release of Ag^+ (Nthunya et al. 2017; Song et al. 2012), resulting in unstable treatment. It was also found that a concentration of Ag^+ higher than that 50 ppm might negatively cause DNA damage in mammalian cells (Ahamed et al. 2008; Kittler et al. 2010). Thus, among those formations of AgNPs on polymer supports was preferred because it is controllable releasing of Ag^+, uniform size distribution and no aggregation with decrease the number of chemical reagents.

Cellulose nanocrystals (CNC) have become one of the main focuses of research in the CNC, which possess many attractive properties such as high specific strength (Abitbol et al. 2016), high surface area, hydrophilicity (George and Sabapathi 2015), biocompatibility (Liu et al. 2017) and ease of surface modification (Putro et al. 2017). CNC has been used to immobilise nanoparticles as biocompatible products (Fu et al. 2018; Hokkanen et al. 2016). An oxidation reaction can produce oxidised-cellulose, which generates small scale cellulose and raises carboxylate groups on the cellulose surface as carboxylated cellulose nanocrystals (cCNC). Carboxyl or aldehyde groups on the cellulose surface have been reported to provide highly dispersed active sites that can connect with nanoparticles in various ways (Fujii et al. 2020; Liu et al. 2019). Carboxylate cellulose nanocrystals (cCNC) has been synthesised by 2,2,6,6-tetramethylpiperidine-1-oxyl radical (TEMPO) oxidation, which occurred at C6 primary hydroxyls to provide carboxyl groups (Ifuku et al. 2009; Uddin et al. 2014) or dialdehyde cellulose at positions C2 and C3 on glucose units (AGU) (Plappert et al. 2018). However, TEMPO-oxidised cellulose involves harmful reducing agents, including hydrazine and sodium borohydride (NaBH4), which exhibit undesirable toxicity and produced many chemical waste products (Ma et al. 2016). Hence, previous studies have reported synthesised carboxylate cellulose nanocrystals by ammonium persulfate oxidation (Jutakridsada et al. 2020). This method has low toxicity, highly oxidising, water-soluble, and low-cost. The synthesis of nanocellulose/silver (Ag-cCNC) nanocomposite has been investigated in many methods (Abdel-Halim and Al-Deyab 2011; Lokanathan et al. 2014; Ma et al. 2016). For instance, Li et al. (2015) (Li et al. 2015) has reported the synthesised Ag on a cellulose substrate by directed hydrothermal on cellulose fibre. They found the uniform particle size, high distribution of AgNPs on the cellulose surface with a high ratio of AgNPs to cellulose at high temperature and hydrothermal reaction pressure, which could be suitable for biomedical application. Also, the particle size of AgNPs in cellulose support can affect their activity in biomedicine (Ahamed et al. 2010)

Thus, in this work, the aim was to prepare carboxylate nanocrystal cellulose (cCNC) from eucalyptus pulp to minimise the process and decrease the number of chemical reagents that immobilise AgNPs on cCNC with stably anchored. The cCNC from the eucalyptus pulp was prepared by using only ammonium persulfate oxidation. Ag-cCNC nanocomposite was produced without adding any chemical reductants or toxic solvents by the hydrothermal method. X-ray diffraction, TGA, TEM-EDX and XPS were used to characterise Ag-cCNC to confirm Ag's presence. The amount of Ag^+ release was determined by ICP-OES analysis. The anticancer HCT 116 (Human colon cancer cell) and SK-MEL-2 (Human Skin Melanoma cell) activity were investigated and compared with cisplatin as a drug cancer treatment. This study contributes to the preparation Ag-cCNC in a simple and environmentally friendly to using natural cellulose with AgNPs as a tumour-killing drug treatment which could be an alternative way to add the value of eucalyptus pulp.

Materials And Methods

Materials

Eucalyptus pulp sheets were supplied by Pheonix Pulp and Paper Public Com. Ltd. Sulfuric acid aqueous solution (96 wt%) and ammonium persulfate (APS) were supplied by RCI-Lab scan (Thailand). Silver nitrate ($AgNO_3$, purity ≥ 99%) were purchase from Sigma Aldrich. Other reagents were purchased from Sigma Aldrich in analytical reagents grade. All of the experimental solutions were prepared using deionised (DI) water.

Synthesis of nanosilver on carboxylate nanocellulose by hydrothermal method

Cellulose nanocrystal (CNC) and Carboxylate cellulose nanocrystal (cCNC) were prepared following the method described in our previous work (Jutakridsada et al. 2020). Briefly, *Eucalyptus* pulp was hydrolysed by mixed with 50 wt% sulfuric acids at 60 °C for 60 min. The hydrolysed sample was washed by deionised water and dried, resulting in CNC. Then, the CNC was modified to produce cCNC by mixing CNC with 1 M ammonium persulfate solution. The mixed solution was maintained at a temperature of 70 $\pm$ 2 °C for 24 h. Then, the mixed solution was separated, and the solid residue was cCNC sample.

Nanosilver on cCNC was prepared in a single step hydrothermal reaction by modified method following Zhang, X. et al.work's (Zhang et al. 2019). In brief, 0.1 g of the cCNC was dissolved entirely with 30 mL of deionised water. Then, cCNC (20 mL) was mixed with 30 mL of silver nitrate solution. The solutions were maintained into a Teflon autoclave of 50 ml and then kept at 140 °C for 4 h. Finally, yellowish solutions were obtained and then separated by centrifuge at 9,000 rpm for 15 min (Hettich Zentrifugen, ROTINA 380R, Germany). The solid phase was Ag-cCNC, which was dried and kept in a desiccator. The different 0.5wt%, 1.0wt% and 1.5wt% $AgNO_3$ concentrations on cCNC were prepared, namely 0.5wt% Ag-cCNC, 1.0wt% Ag-cCNC, and 1.5wt% Ag-cCNC, respectively.

Characterisation

X-ray diffraction (XRD) measurements

Crystal structure of CNC, cCNC, various Ag-cCNC samples were determined by X-ray diffraction (Bruker D8 Advance, Germany). The XRD pattern of all samples was analysed using Ni-filtered Cu Kα radiation (λ = 1.5406 Å), operating at 40 kV and 30 mA. The CNC, cCNC and all Ag-cCNC samples were scanned within 2θ range of 10–80°. All samples' crystal profile was drawn using Mercury software 4.3.1 (The Cambridge Crystallographic Data Centre Cambridge, UK).

Fourier transform infrared spectroscopy (FTIR)

The functional chemical group of CNC, cCNC, Ag-cCNC were measured by FT-IR spectrometer (Bruker, Germany). Ten mg of samples were pressed into an acrylic mould with a diameter of 10 mm. FTIR spectra were recorded in spectral wavelength between 600 and 4000 cm^{-1} with a 4 cm^{-1} of resolution.

Thermal Gravimetric Analysis (TGA)

The thermal stability of the catalyst is an essential criterion for application in practice. The thermal decomposition of CNC, cCNC and various Ag-cCNC samples was characterised by TGA analysis (TGA 50, Shimadzu, Japan). A 200-mg sample of the material was heated in a temperature range of 35-700°C at a heating rate of 10 °C /min under nitrogen flow.

X-ray photoelectron spectra (XPS)

X-ray photoelectron spectra (XPS) were used to analyse the molecular binding with an X-ray photoelectron spectrometer (AXIS Ultra DLD, Kratos Co., England) with monochromatic Al Kα (1486.6 eV) radiation as the excitation source. The binding energy charge was corrected to 284.6, 368.2,531.5 eV for C 1s, Ag 3 d, and O 1s.

Transmission electron microscopy (TEM-EDX)

The morphology of various Ag-cCNC concentrations was imaged using Transmission electron microscopy energy-dispersive X-ray spectroscopy (Tecnai^2 G^2 20, FEI, USA), and the energy dispersive X-ray spectrometers (EDX), (X-Max in the FESEM and INCAxsight in the TEM, Oxford instrument, UK). The samples were prepared by dispersed into ethanol in a ratio of 1:10 (samples: ethanol). Ten µl of dispersed samples were added to the carbon-coated electron microscopy grid. Then, the samples were observed at 100 kV using a transmission electron microscope.

Particle size distribution

The particle size distribution of various Ag-cCNC concentrations was determined by Zetasizer Nano ZS instrument (Malvern Instruments, Malvern, UK). All Ag-cCNC samples were dispersed deionised water (DI). One millilitre of the samples was inserted into a single-use disposable polystyrene cuvette DTS0012 (Malvern Panalytical, Malvern, UK). The particle size distribution (PSD) was measured at 25 °C in three repeated measurements.

UV-Vis spectra

UV–vis spectra were performed on an Agilent UV–vis spectrophotometer (Agilent Technologies, USA) in the range of 200–800 nm with a resolution of 2 nm. Two mL of Ag-cCNC solution samples were placed in a 1 cm thick quartz cuvette, and spectra were recorded at room temperature.

Ag^+ Release Behavior

This method was adapted from Li J et al (2019) (Li et al. 2019) with a minor modification. In brief, 0.05 g of 1.5wt%Ag-cCNC sample was mixed with 50 mL of DI water in a screw cap centrifuge tube and incubated at a temperature of 37 °C. The mixed sample was centrifuged at 9,000 rpm every 48 h. The liquid phase was separated to determine the amount of Ag^+ release. The residual solid phase was added into 50 ml of distilled water in the other tube container and kept at 37 °C. This procedure was conducted on a 48 h interval for 32 days. The Ag^+ concentrations in the solutions were analysed using ICP-OES (ICP-OES; 5110, Agilent, USA). Before analysis, the ICP-ES instrument was calibrated silver concentration by the standard silver nitrate solution of different concentrations.

Cytotoxicity test

Cell lines and culture

HCT116 (human colon cancer, ATCC#CCL-247) cell and SK-MEL-2 (Skin cell melanoma cancer cell) line was cultured in DMEM. The media were supplemented with 10% fetal bovine serum (FBS), 100 units/ml penicillin, and 100 µg/ml streptomycin. The cell lines were incubated at 37 °C with 95% air and 5% CO_2 and reached approximately 80% confluent before use.

Cell cytotoxicity by NR assay

As previously described, the cytotoxicity activities of CNC and 1.5wt% Ag-cCNC and NR assay (Pocasap et al. 2018). Briefly, HCT116 and SK-MEL-2 cells at 3.5×105 cells/ml were seeded into 96-well plates. Then, cells were

treated with various concentrations of samples for 24 h. The cells were washed with PBS and incubated with neutral red (final concentration of 50 µg/ml) for 2 h at 37 °C. The supernatant was removed, and the neutral red incorporated inside the cell was lysed by 0.33% HCl in isopropanol. The absorbance of neutral red dye was measured at 537 nm (with 660 nm as a reference wavelength) using EnSight multimode plate reader (PerkinElmer, Waltham, MA, USA). Antiproliferative activity was calculated as a percentage compared to the untreated cells and expressed as mean ± SD.

Results And Discussion

Characterisation of CNC, cCNC and Ag-cCNC

XRD of the synthesised samples was determined. Figure 1 illustrates X-ray diffraction (XRD) patterns of CNC, cCNC and various Ag-cCNC concentrations. All samples present the diffraction peaks at approximately 16°, 22° and 34° corresponding to (110), (200) and (004), respectively are associated with cellulose type I as its natural form. In case of Ag-cCNC samples, there are the diffraction peaks at 38°, 44°, 64° and 77° assigning to the (111), (200), (220) and (311) plane of face centred cubic (FCC) silver (Ag) (Han et al. 2016).

Figure 2 shows FTIR spectra of CNC, cCNC and various Ag-cCNC concentrations. The appearance peak at 1051, 1651, 1730, 2912 and 3350 cm^{-1} were found in all samples. The peak at 1051 cm^{-1} was associated with C-O's bending vibration corresponding to the hydroxyl group in a cellulose structure. The CNC and cCNC show a strong peak while the Ag-cCNC displayed a small peak. The decreased peak was found in Ag-cCNC sample. This result was due to the fact that the hydroxyl group may disrupt during the hydrothermal reaction.

The peak at 1651 cm^{-1} was attributed to the OH group's bending scribable to aldehyde or ketone groups (Castro-Guerrero and Gray 2014), indicating no aldehyde or ketone groups occurred in the CNC. Therefore, their occurrence of bands at 1730 cm^{-1} indicated that CNCs had experienced carboxylation. An appearance peak at 1614 cm^{-1} of cCNC assigned to the carboxylate groups (-COO), whereas this spectrum disappeared in Ag-cCNC sample. This possible explanation is that the carboxylate group on cCNC acts as an active site for silver adsorption, which the carboxylate groups might involve the redox reaction.

The peak at 2912 cm^{-1} was ascribed to the stretching vibration of C-H. The peak at 3350 cm^{-1} was associated with the hydrogen bond stretching of OH groups. It can be noticed that the spectra of Ag-cCNC at this peak had lower absorbance than that of CNC and cCNC. The possible explanation is that the hydroxyl groups (OH) could be induced to interact with the Ag nanoparticles' surface. Furthermore, the absorption band attributed to the hydrogen bond stretching vibration in Ag-cCNC was shifted, which could be explained by the interaction of OH groups with the Ag nanoparticles surface.

Figure 3 shows TGA curves of CNC, cCNC and various Ag-cCNC concentrations in N_2. The major weight loss of CNC and cCNC was in the range of 150–550°C, while Ag-cCNC samples were at 250-450°C. This result showed higher thermal stability of the materials in the presence of AgNPs. Also, the percentage yield of the silver content in the composite fibers was calculated. The %yield of 17.7, 23.3 and 28.0 for 0.5wt%, 1.0wt% and 1.5wt% Ag-cCNC, respectively.

According to X-ray photoelectron spectroscopy (XPS) results, the chemical composition and bonding of CNC, cCNC, 0.5wt%Ag-cCNC, 1.0wt% Ag-cCNC and 1.5wt% were scanned in the range of 0-1100 eV (as in fig.1s in supplementally data). The essential spectra of each sample are shown in Figure 4 (a)-(e). The XPS spectra of all

samples show binding energy in three regions, Ag 3d, C 1s and O 1s, with different ranges. At Ag 3d region, the two peaks with binding energies of Ag 3d 3/2 and Ag 3d 5/2 at 366.2 and 372.2 eV, respectively, were recognised in all Ag-cCNC concentrations. In contrast, there were no two peaks in CNC and cCNC samples. Two prominent peaks indicate Ag 3d 3/2 and Ag 3d 5/2, attributed to Ag^0 (Ramstedt and Franklyn 2010). The energy gap between Ag 3d 3/2 and Ag 3d 5/2 was ca. 6 eV, indicating a splitting of the two peaks of Ag 3d can be due to the spin–orbit coupling. This result confirmed by the existence of Ag^0 state on the cellulose surface. Similarly, Dong et al. (2015) has reported the silver zero-valence on silver-reinforced cellulose hybrids with the associate XPS peak at 368.0 and 373.9 eV. Also, Murray et al. (2005) proposed that Ag(0) in nanosilver wire could play an essential role in Ag^+ release, which could be applied for antibacterial and anticancer treatment (Islam et al. 2018; Vijayakumar et al. 2019). The appearance of silver was in good agreement with XRD analysis.

At C1s region, it can be noticed four peaks occurred at 283.1, 284.6 and 286.1 eV, corresponding to the carbon of alkyl (C-C/C-H), alcohol (C-OH), ether (C-O-C), respectively, in all samples. Also, the peak of carboxyl carbon (C = O) at 287.9 eV was found in all cCNC samples. A surface-modified CNC process could cause this. Interestingly, the peak of ether (C-O-C) and carboxyl carbon (C = O) at 286.9 and 288.0 eV of all Ag-cCNC sample was shifted a little to the higher binding energy in comparison with cCNC sample, and it could confirm that the carboxyl acts as nucleation sites for Ag NPs loading onto cCNC.

At O1s region, the spectra of oxygen making single bonds carbon (C-O), oxygen making a double bond with carbon C=O and surface hydroxyl groups (O–H) (O in H_2O)) were found in all samples. Similarly, there was a minor shift in all Ag-cCNC, which agrees with Ag's presence on the surface of cCNC.

Based on XPS results, the possible forming of Ag-cCNC was proposed, as shown in Figure 4. The reaction was composed of two steps; surface-modified by Ammonium persulfate reagent and hydrothermal reaction. Firstly, C4 hydroxyl group in β-d-glucopyranoside on CNC surface was oxidised to become carboxylate cellulose nanocrystal (cCNC) by ammonium persulfate reagent, providing a lot of carboxyl carbon (C = O) and also OH group on the end of cCNC (as mentioned in XPS result). This mechanism has been reported in previous work (Jutakridsada et al. 2020). Secondly, Ag-cCNC was synthesised by a one-step hydrothermal reaction. During the hydrothermal reaction, the redox reaction between cCNC and $AgNO_3$ occurred, which cCNC can act as a reducing agent to reduce Ag^+ into Ag (Zhang et al. 2019). Under high temperature and pressure, the absorbed Ag^+ was reduced by OH and carboxyl groups and formed Ag's initial nucleation site, and silver nanoparticle would be stably anchored at the carboxylate groups on the surface of cCNC (Wu et al. 2014). A similar result has been reported by Zhang et al. (2019), which prepared Ag onto TEMPO-oxidised nanocelluloluse by the hydrothermal reaction, resulting in the attached Ag on oxidised nanocelluloluse surface. However, they synthesised Ag on oxidised-nanocelluloluse with three steps; TEMPO-oxidised nanofibrillated cellulose, dialdehyde nanofibrillated cellulose and deposition of Silver Nanoparticles onto dialdehyde nanofibrillated cellulose. While in this work, Ag-cCNC was produced in two steps; APS-oxidised nanocellulose and Ag-doping using only $AgNO_3$ by hydrothermal reaction. This result shows Ag^0 achievement on cellulose nanocrystal with a few steps and number of reductants or stabilisers, enabling use in biomedical application with an environmentally friendly approach.

Morphology of Ag-cCNC

Figure 6 shows TEM images of various Ag-cCNC concentrations—the aggregated black particles was silver particle interspaces of cCNC , which were noticed that the more silver nanoparticles, the higher Ag concentrations. Ag particles' high distribution on cCNC surface was observed with the range of 5 – 50 nm. The average Ag particle

size was at ca 21.96 ± 8.04, 18.92 ± 7.80, and 15.79 ± 6.59 am for 0.5,1.0 and 1.5wt%Ag-cCNC, respectively (in Table S.1 supplementary matertials). According to the EDX analysis (Fig 5d, 5e, and 5f. The EDX spectra show a silver element peak at 4, 23, 25 keV. Small Ag particles with fair distribution offered high catalytic activity, generating ROS as an essential anticancer or antibacterial mechanism (Zhang et al. 2019).

The particle size distribution of various Ag-cCNC concentrations was measured using Zetasizer Nano ZS instrument. Figure 7 (a) –(c) shows a size distribution histogram of various Ag-cCNC concentrations. There were three ranges of particles sized 4.84-11.70, 43.82-78.82 and 396.10-712.40 nm for 0.5wt% Ag-cCNC (Figure 6(a)) and 4.85-7.53, 37.84-68.06 and 295.30-531.20 nm for 1.0 wt% Ag-cCNC (Figure 6(b)), whereas it was two regions; 6.50-10.10 and 141.80-190.10 nm for 1.5 wt% Ag-cCNC (Figure 6(c)). The majority of particle sizes of various Ag-cCNC concentrations was in the range of a few hundred nanometers. Comparison, in the majority range, the particle size significantly decreased when the concentration of Ag increased. At a low concentration of silver nitrate, it could have fewer Ag ion deposition on hydroxyl groups in cCNC. The cluster of cCNC was in the main particles. This heterogeneous structure leads to the non-uniform breakup of carboxylated cellulose nanocrystals (cCNC), resulting in a low distribution of silver nanoparticles (AgNPs) in cellulose substrate. In contrast to, at high concentration of Ag, this may be the Ag^{+} was randomly selected attach surface of cCNC, and this could be decreased cluster of cCNC during the hydrothermal reaction. This result agrees with the Sadanand et al. (2017) work's, who found the average size of Ag NPs particle decreased with an increase of $AgNO_3$ solution concentration prepared by hydrothermal method.

UV–Vis Spectra Analyzing Nanoparticle Assembly

UV-Vis Spectrophotometer was used to measure the excitation of the surface plasmon resonance (SPR) band of nanosilver particles, which confirm the presence of Ag NPs on cCNC surface. Figure 7 shows the UV-Vis spectra of cCNC and various Ag-cCNC concentrations in the wavelength of 250-600 nm. The result presents the absorption peak at about 412 nm in all Ag-cCNC samples, while there is no spectrum at this wavelength in the cCNC sample. During the Ag-cCNC synthesis process, the Ag-cCNC solutions displayed a colour change from milk-white to dark brown, which shows nanosilver particle formation. The colour change occurs because the free electrons were moved from valence band to conduction band (Singh et al. 2013) at the surface of the nanoparticles, and then, the oscillation of their electron in resonance was given a brown colour with a unique surface plasmon resonance (SPR) band (Sotiriou 2013). This result is because of the SPR effect induced by Ag NPs. Also, the absorbance significantly increased when the percentage of Ag NPs in cCNC increased.

Table 1 shows the %yield, average particle size and silver particle size of Ag-doping on cCNC. The as-prepared 1.5wt%Ag-cCNC produced a higher %yield with a similar range of Ag particle size and average Ag particle to the other works, which could benefit their catalytic activity and industrial proposed. Most important, the controllable release could be the key to the biomedical application due to the high Ag dose(> 50 ppm) that can damage a human cell.

Table 1 comparison between %yield, average particle size and silver particle size of Ag-doping on cCNC composite with hydrothermal reaction and the other methods.

Composite material	Method	%yield of AgNPs	Range of silver particle sizes (nm)	Average silver particle size (nm)	References
Bacterial cellulose/Silver nanoparticles	Immersed $AgNO_3$	25.0	70 - 100	85	(de Santa Maria et al. 2009)
Cellulose/ Silver nanoparticles	TEMPO oxidation/Hydrothermal	25.3	-	9.8	(Fujii et al. 2020)
Dialdehyde Nanofibrillated Cellulose/Silver Nanoparticle	Ultrasonication at 80 °C	1.79	8 - 37	16.63	(Li et al. 2019)
Cellulose fibre/ Silver nanoparticles	Hydrothermal at 80 °C	2.4	6.5 - 20	7.2-12.5	(Li et al. 2015)
Cellulose/silver nanoparticles	Hydrothermal at 80 °C	4.9	8 - 48	18.6	(Wu et al. 2012)
Cellulose/silver nanoparticles	Microwaves assist and Hydrothermal at 160 °C	23.1	-	16	(Fu et al. 2018)
1.5%wt Ag-cCNC	Hydrothermal at 140 °C	28.0	4.87 - 37.31	15.79 ± 6.59	This work

Control releasing

The noble metal nanoparticles such as silver (Ag), Gold (Au), Zinc oxide (ZnO), and Titanium dioxide (TiO_2) are most promising in the anticancer treatment (Arjunan et al. 2016; Murugan et al. 2016; Sivakumar et al. 2018; Vijayan et al. 2019). However, the high dose of NMNPs can cause side-effects on the human cell; for example, Greulich et al. (2012) reported the toxic effect of silver nanoparticle in the range of 12.5 – 50 ppm on the human cell. A high amount of silver nanoparticle can produce many oxidised reactive oxygen species (ROS), directly inhibiting the human cell membrane and leading to death (Johnston et al. 2010). Sambale et al. (2015) have also suggested similar results, but Ag^+ in the range of 10-40 ppm could affect a human cell.

Recently, silver nanoparticles could achieve excellent biomedical applications such as antibacterial and anticancer but lower concentration at 50 ppm for silver nanoparticle (40 ppm for Ag^+), which are not harmful to human cells. (Mohamed et al. 2020). However, it has been reported that a high concentration of Ag NPs has cytotoxicity on a human cell; especially, the Ag NPs size with a diameter of 100-160 mm, lengths of 1.5 – 25 µm could have cytotoxic effects on human lung cells (Sankar et al. 2013). Thus, the immobilised silver nanoparticles on cellulose could be the alternative way to control the releasing rate of Ag NPs and form Ag zero valence on cCNC surface. The amount of Ag ions were measured by ICP-OES analysis. Figure 9 presents the number of Ag^+ release rates and cumulative Ag^+ of 1.5wt% Ag-cCNC in DI water for 32 days. As can be seen, the highest Ag^+ releasing of 5.38±0.244 ppm was found in the first two days. During 2-32 days, Ag^+ releasing fluctuated in the range of 2.76 ± 0.10–1.24 ± 0.05 ppm (0.10±0.06 –0.05±0.01%). The cumulative Ag^+ releasing was approximately 38.18±2.35 ppm (1.47±0.81 %) for 32 days. Table 2 shows the concentration of Ag^+on cCNC surface, amount and % Ag^+ release at 32 days in all Ag-cCNC samples.

As reported by Sambale, F. et al. (Sambale et al. 2015), Ag^+ ion is not harmful to human cells at a concentration below 40 ppm; in our result, the total Ag^+ release was 38.18±2.35 ppm in 32 days, which could not damage human cells. The linear fitting of the total release of Ag^+ shown in Figure 6. The linear fitting equation is following the below equation:

$$y = 0.041x + 0.1602 \quad (1)$$

where Y is the total release of Ag^+ (%), x is the period of releasing time (days), and R^2 is the correlation coefficient.

As following to our Ag^+ releasing equation (1), the average release per 2 days of Ag^+ was approximate 0.81 ± 0.57% (2.46 ± 1.15 ppm) (0.41%/day), while Maneerung et al. (2008) reported the initial Ag^+ release rate from the silver nanoparticle impregnated on bacterial cellulose at approximately 10.7%/day. Zhao et al. (2017) also presented a 12.2%/day releasing of silver Nanoparticles Loaded Graphene Oxide. Our results were much lower than that of literature works. Ag^+ of Ag-cCNC has displayed a slow and controllable release of Ag^+ from the nanoscale substrates, which could be desired the drug's release rate or active ingredient gradually over the day (Yun et al. 2015) without toxic to human cells. Table 2 shows the concentration of Ag^+on cCNC surface, amount and % Ag^+ release at 32 days. The maximum amount of Ag^+ on cCNC and total Ag^+ release was occurred at 1.5wt%cCNC sample wheras it was the lowest in %releasing.

In our work, the Ag^+ would be released entirely from Ag-cCNC approximately in 245 days. It offers a long-term Ag^+ releasing that could cause a strong interaction between cCNC and silver nanoparticles by the hydrothermal method. Compare to Zhao et al. (2017) work's, and they reported the released Ag^+ at 97.0% silver nanoparticles (AgNPs) on graphene oxide (GO) nanocomposite (GO-Ag) by microwave synthesiser for 16 days. It could be an excellent suggestion to use the hydrothermal reaction to deposition Ag NPs on cellulose. Since the controlled Ag^+ release from cellulose surface shown a long-term Ag^+ releasing, which would be useful in the application on the biomedical field such as chemotherapy medication, skin plaster (Yi et al. 2019), surgical sutures (Guambo et al. 2020), and wound dressings (Gupta et al. 2020) and other advanced biomaterials (George et al. 2019; Hickey and Pelling 2019; Mandal et al. 2017). This may not need a high concentration dose, but it should be a long term activity.

Table 2 Ag^+ concentration on cCNC and total releasing of Ag^+ in 32 days

Sample	The concentration of Ag^+ on cCNC (ppm)	Total Ag^+ releasing in 32 days (ppm)	% Total Ag^+ releasing in 32 days (%)
0.5%wt Ag-cCNC	805.66 ± 2.41	19.65 ± 0.766	2.44 ± 0.07
1.0%wt Ag-cCNC	2062.18 ± 6.18	32.79 ± 1.27	1.59 ± 0.05
1.5%wt Ag-cCNC	2445.06 ± 7.33	39.16 ± 1.52	1.53 ± 0.06

Antitumour activity of Ag-cCNC against HCT116 and SK-MEL-2

Figure 10 (a) and (b) shows the percentage of viability of HCT116 human colon cancer cell line and SK-MEL-2 Human Skin Melanoma cell line, respectively, with various doses of cCNC and 1.5wt% Ag-cCNC, cisplatin as a chemotherapy medication, untreated cell and 1% DMSO as solvent control at treatment times of 24 h. It can be noticed that there was no anticancer activity in cCNC sample with about 100% viability at all concentrations in both HCT 116 and SK-MEL-2 Cell lines. While 1.5wt% Ag-cCNC sample, it inhibited cell growth and viability of HCT116 human colon cancer cell line and SK-MEL-2 Human Skin Melanoma cell line with 35% and 20%viability, respectively, at the dose of 200 µg/mL and it had no activity in both cancer cell at a dose of 50 and 100 µg/mL. Comparison to cisplatin ($[Pt(NH_3)_2Cl_2]$) as well-known high-efficient cancer chemotherapy, 1.5wt% Ag-cCNC sample with the dose of 200 µg/mL obtained higher 15%inhibition HCT 116 cancer cell than that of Cisplatin. In contrast, cisplatin performed a larger 15%inhibition SK-MEL-2 Human Skin Melanoma cancer cell than 1.5wt% Ag-cCNC sample with a dose of 200 µg/mL. This may be due to the different biological structure and DNA in HCT 116 cells and SK-MEL-2 cells (Taylor et al. 2019). Also, It has been reported that cisplatin has an overall cure rate exceeds 90% (Dasari and Tchounwou 2014), which inhibits DNA synthesis or inhibition of cell growth.

As shown in Figure 11, the graphical mechanism of Ag-cCNC attack on a cancer cell, Ag-cCNC could release Ag^+ from Ag nanoparticle on cCNC surface, which generate the ROS to penetrate the cancer cell membrane and induce cancer cell death. ROS production is an important mechanism behind Ag nanoparticles' anticancer effect (Zhang et al. 2016). This result can be confirmed the anticancer activity of Ag-cCNC sample. The physical properties of Ag-cCNC such as size, Ag releasing, morphology is critically performed of anticancer activity. The smaller size of Ag-cCNC (in the range of 5-190 nm), the higher cytotoxicity effects on both cancer cells. This is because a small Ag-cCNC particle size could attach to the cancer cell, where Ag nanoparticles would release Ag^+ and generate the ROS to destroy the cell (Chugh et al. 2018). Also, it was reported that the positively charged Ag^+ ions could create higher activity than negative charges due to the ionic interaction between negatively charged cell membrane surfaces (Zhang et al. 2019). This leads to cell membrane leakage and penetration into cancer cells. As consistent with cytotoxicity assay, antiproliferative assay results revealed that 1.5wt% Ag-cCNC sample inhibited cell growth and viability of all cancer cell lines in a dose-dependent manner.

However, in this work, the anticancer activity of Ag-cCNC on HCT-116 colon cancer cells shows higher efficiency than that of SK-MEL-2 Human Skin Melanoma cells, whereas cisplatin demonstrated the opposite results. Practically, the application of Ag-cCNC to anticancer may be suitably used in skin cell due to its heterogeneous phase. It can target a healing point in skin cell activity that could perform high efficacy and low side effect. Further study needs to be in clinical testing.

Conclusion

In this study, Ag-cCNC was successfully fabricated by APS-oxidised cellulose and hydrothermal reaction, which used two steps and minimised the chemical reagent as reductants or stabilisers; APS for surface-modified and $AgNO_3$ for the hydrothermal reaction. XPS results showed the interaction between Ag NPs on cCNC. TEM-EDX result revealed the aggregated black particles as silver particle interspaces of cCNC, with Ag particles' well-distribution on cCNC surface with ca 15 nm. The particle size of Ag-cCNC composite significantly decreased with an increased in Ag dose. The maximum Ag-doping of 28.0% yield was in 1.5wt%Ag-cCNC. The most petite composite sized of 141.80-190.10 nm was also obtained at 1.5wt% Ag-cCNC. The average release rate of Ag^+ from the 1.5wt% Ag-cCNC was at 2.76±0.10 – 1.24±0.05 ppm (0.1-0.2%) per 2 days, and the maximum accumulation of Ag^+ was at 38.18±2.35 ppm (1.47±0.81 %) for 32 days, which showed longer release. Also, 1.5wt% Ag-cCNC with 200 200 µg/mL showed antitumour HCT 116 (Human colon cancer cell) and SK-MEL-2 Human Skin Melanoma cell) activity with 35±4.04% and 20±7.68%, respectively. The result shows high efficacy in both anticancer cells, comparing to cisplatin as an anticancer reagent. This work could prepare an antitumour drug with fewer process steps and contribute to the alternative way to use and value-add natural cellulose from Eucalyptus pulp.

Declarations

Acknowledgement

We gratefully acknowledge Farm Engineering and Automatic Control Technology Research group (FEAT Group), Applied Engineering for Important Crops of the North East Research group (AENE Group), and the Graduate School at Khon Kaen University for student financial support. We are also grateful to LUT University for providing characterisation instruments.

Declarations

Funding: The authors did not receive support from any organisation for the submitted work.

Conflicts of interest/Competing interests: The authors have no conflicts of interest to declare that they are relevant to this article's content.

References

Abdel-Halim E, Al-Deyab SS (2011) Utilization of hydroxypropyl cellulose for green and efficient synthesis of silver nanoparticles Carbohydrate polymers 86:1615-1622

Abitbol T et al. (2016) Nanocellulose, a tiny fiber with huge applications Current Opinion in Biotechnology 39:76-88 doi:https://doi.org/10.1016/j.copbio.2016.01.002

Ahamed M, AlSalhi MS, Siddiqui MKJ (2010) Silver nanoparticle applications and human health Clinica Chimica Acta 411:1841-1848 doi:https://doi.org/10.1016/j.cca.2010.08.016

Ahamed M, Karns M, Goodson M, Rowe J, Hussain SM, Schlager JJ, Hong Y (2008) DNA damage response to different surface chemistry of silver nanoparticles in mammalian cells Toxicology and Applied Pharmacology 233:404-410 doi:https://doi.org/10.1016/j.taap.2008.09.015

Arjunan N, Kumari HL, Singaravelu CM, Kandasamy R, Kandasamy J (2016) Physicochemical investigations of biogenic chitosan-silver nanocomposite as antimicrobial and anticancer agent Int J Biol Macromol 92:77-87 doi:10.1016/j.ijbiomac.2016.07.003

Castro-Guerrero CF, Gray DG (2014) Chiral nematic phase formation by aqueous suspensions of cellulose nanocrystals prepared by oxidation with ammonium persulfate Cellulose 21:2567-2577

Chugh H, Sood D, Chandra I, Tomar V, Dhawan G, Chandra R (2018) Role of gold and silver nanoparticles in cancer nano-medicine Artificial cells, nanomedicine, and biotechnology 46:1210-1220 doi:10.1080/21691401.2018.1449118

Dasari S, Tchounwou PB (2014) Cisplatin in cancer therapy: molecular mechanisms of action European journal of pharmacology 740:364-378

de Martel C, Georges D, Bray F, Ferlay J, Clifford GM (2020) Global burden of cancer attributable to infections in 2018: a worldwide incidence analysis The Lancet Global Health 8:e180-e190 doi:10.1016/S2214-109X(19)30488-7

de Santa Maria LC, Santos ALC, Oliveira PC, Barud HS, Messaddeq Y, Ribeiro SJL (2009) Synthesis and characterization of silver nanoparticles impregnated into bacterial cellulose Materials Letters 63:797-799 doi:https://doi.org/10.1016/j.matlet.2009.01.007

Dong Y-Y, Fu L-H, Liu S, Ma M-G, Wang B (2015) Silver-reinforced cellulose hybrids with enhanced antibacterial activity: synthesis, characterization, and mechanism RSC Advances 5:97359-97366 doi:10.1039/C5RA19758A

Fu L-H, Gao Q-L, Qi C, Ma M-G, Li J-F (2018) Microwave-Hydrothermal Rapid Synthesis of Cellulose/Ag Nanocomposites and Their Antibacterial Activity Nanomaterials 8:978

Fujii Y, Imagawa K, Omura T, Suzuki T, Minami H (2020) Preparation of Cellulose/Silver Composite Particles Having a Recyclable Catalytic Property ACS Omega 5:1919-1926 doi:10.1021/acsomega.9b03634

Gaumet M, Vargas A, Gurny R, Delie F (2008) Nanoparticles for drug delivery: the need for precision in reporting particle size parameters European journal of pharmaceutics and biopharmaceutics 69:1-9

George D, Maheswari PU, Begum KMS (2019) Synergic formulation of onion peel quercetin loaded chitosan-cellulose hydrogel with green zinc oxide nanoparticles towards controlled release, biocompatibility, antimicrobial and anticancer activity International journal of biological macromolecules 132:784-794

George J, Sabapathi SN (2015) Cellulose nanocrystals: synthesis, functional properties, and applications Nanotechnol Sci Appl 8:45-54 doi:10.2147/NSA.S64386

Ghasemzadeh H, Mahboubi A, Karimi K, Hassani S (2016) Full polysaccharide chitosan-CMC membrane and silver nanocomposite: synthesis, characterization, and antibacterial behaviors Polymers for Advanced Technologies

27:1204-1210 doi:https://doi.org/10.1002/pat.3785

Greulich C, Braun D, Peetsch A, Diendorf J, Siebers B, Epple M, Köller M (2012) The toxic effect of silver ions and silver nanoparticles towards bacteria and human cells occurs in the same concentration range RSC Advances 2:6981-6987 doi:10.1039/C2RA20684F

Guambo MPR et al. (2020) Natural Cellulose Fibers for Surgical Suture Applications Polymers 12:3042

Gupta A et al. (2020) Synthesis of Silver Nanoparticles Using Curcumin-Cyclodextrins Loaded into Bacterial Cellulose-Based Hydrogels for Wound Dressing Applications Biomacromolecules 21:1802-1811 doi:10.1021/acs.biomac.9b01724

Han Y, Wu X, Zhang X, Zhou Z, Lu C (2016) Reductant-free synthesis of silver nanoparticles-doped cellulose microgels for catalyzing and product separation ACS Sustainable Chemistry & Engineering 4:6322-6331

Harra J et al. (2012) Size-controlled aerosol synthesis of silver nanoparticles for plasmonic materials Journal of Nanoparticle Research 14:870 doi:10.1007/s11051-012-0870-0

Hickey RJ, Pelling AE (2019) Cellulose biomaterials for tissue engineering Frontiers in Bioengineering and Biotechnology 7:45

Hokkanen S, Bhatnagar A, Sillanpää M (2016) A review on modification methods to cellulose-based adsorbents to improve adsorption capacity Water Research 91:156-173 doi:https://doi.org/10.1016/j.watres.2016.01.008

Ifuku S, Tsuji M, Morimoto M, Saimoto H, Yano H (2009) Synthesis of Silver Nanoparticles Templated by TEMPO-Mediated Oxidized Bacterial Cellulose Nanofibers Biomacromolecules 10:2714-2717 doi:10.1021/bm9006979

Islam MS, Akter N, Rahman MM, Shi C, Islam MT, Zeng H, Azam MS (2018) Mussel-inspired immobilization of silver nanoparticles toward antimicrobial cellulose paper ACS Sustainable Chemistry & Engineering 6:9178-9188

Johnston HJ, Hutchison G, Christensen FM, Peters S, Hankin S, Stone V (2010) A review of the in vivo and in vitro toxicity of silver and gold particulates: particle attributes and biological mechanisms responsible for the observed toxicity Critical reviews in toxicology 40:328-346 doi:10.3109/10408440903453074

Jutakridsada P, Pimsawat N, Sillanpää M, Kamwilaisak K (2020) Olive oil stability in Pickering emulsion preparation from eucalyptus pulp and its rheology behaviour Cellulose 27:6189-6203 doi:10.1007/s10570-020-03206-6

Kittler S, Greulich C, Diendorf J, Köller M, Epple M (2010) Toxicity of Silver Nanoparticles Increases during Storage Because of Slow Dissolution under Release of Silver Ions Chemistry of Materials 22:4548-4554 doi:10.1021/cm100023p

Li J et al. (2019) Controlled Release and Long-Term Antibacterial Activity of Dialdehyde Nanofibrillated Cellulose/Silver Nanoparticle Composites ACS Sustainable Chemistry & Engineering 7:1146-1158 doi:10.1021/acssuschemeng.8b04799

Li R, He M, Li T, Zhang L (2015) Preparation and properties of cellulose/silver nanocomposite fibers Carbohydrate Polymers 115:269-275 doi:https://doi.org/10.1016/j.carbpol.2014.08.046

Litwin MS, Tan H-J (2017) The Diagnosis and Treatment of Prostate Cancer: A Review JAMA 317:2532-2542 doi:10.1001/jama.2017.7248

Liu H et al. (2017) Facile fabrication of redox/pH dual stimuli responsive cellulose hydrogel Carbohydrate polymers 176:299-306

Liu S, Zhu Y, Wu Y, Lue A, Zhang C (2019) Hydrophobic modification of regenerated cellulose microparticles with enhanced emulsifying capacity for O/W Pickering emulsion Cellulose 26:6215-6228

Lokanathan AR, Uddin KMA, Rojas OJ, Laine J (2014) Cellulose nanocrystal-mediated synthesis of silver nanoparticles: role of sulfate groups in nucleation phenomena Biomacromolecules 15:373-379

Ma P, Jiang L, Yu M, Dong W, Chen M (2016) Green Antibacterial Nanocomposites from Poly(lactide)/Poly(butylene adipate-co-terephthalate)/Nanocrystal Cellulose–Silver Nanohybrids ACS Sustainable Chemistry & Engineering 4:6417-6426 doi:10.1021/acssuschemeng.6b01106

Mandal B, Rameshbabu AP, Soni SR, Ghosh A, Dhara S, Pal S (2017) In Situ Silver Nanowire Deposited Cross-Linked Carboxymethyl Cellulose: A Potential Transdermal Anticancer Drug Carrier ACS Applied Materials & Interfaces 9:36583-36595 doi:10.1021/acsami.7b10716

Maneerung T, Tokura S, Rujiravanit R (2008) Impregnation of silver nanoparticles into bacterial cellulose for antimicrobial wound dressing Carbohydrate Polymers 72:43-51 doi:https://doi.org/10.1016/j.carbpol.2007.07.025

Mohamed DS, Abd El-Baky RM, Sandle T, Mandour SA, Ahmed EF (2020) Antimicrobial Activity of Silver-Treated Bacteria against other Multi-Drug Resistant Pathogens in Their Environment Antibiotics (Basel) 9:181 doi:10.3390/antibiotics9040181

Murray B, Li Q, Newberg J, Menke E, Hemminger J, Penner R (2005) Shape-and size-selective electrochemical synthesis of dispersed silver (I) oxide colloids Nano Letters 5:2319-2324

Murugan K et al. (2016) Hydrothermal synthesis of titanium dioxide nanoparticles: mosquitocidal potential and anticancer activity on human breast cancer cells (MCF-7) Parasitol Res 115:1085-1096 doi:10.1007/s00436-015-4838-8

Nthunya LN et al. (2017) Greener Approach To Prepare Electrospun Antibacterial β-Cyclodextrin/Cellulose Acetate Nanofibers for Removal of Bacteria from Water ACS Sustainable Chemistry & Engineering 5:153-160 doi:10.1021/acssuschemeng.6b01089

Plappert SF et al. (2018) Transparent, Flexible, and Strong 2,3-Dialdehyde Cellulose Films with High Oxygen Barrier Properties Biomacromolecules 19:2969-2978 doi:10.1021/acs.biomac.8b00536

Pocasap P, Weerapreeyakul N, Thumanu K (2018) Structures of isothiocyanates attributed to reactive oxygen species generation and microtubule depolymerization in HepG2 cells Biomedicine & pharmacotherapy = Biomedecine & pharmacotherapie 101:698-709 doi:10.1016/j.biopha.2018.02.132

Putro JN, Kurniawan A, Ismadji S, Ju Y-H (2017) Nanocellulose based biosorbents for wastewater treatment: study of isotherm, kinetic, thermodynamic and reusability Environmental nanotechnology, monitoring & management 8:134-149

Qiao W, Wang B, Wang Y, Yang L, Zhang Y, Shao P (2010) Cancer therapy based on nanomaterials and nanocarrier systems Journal of Nanomaterials 2010

Ramstedt M, Franklyn P (2010) Difficulties in determining valence for Ag0 nanoparticles using XPS—characterization of nanoparticles inside poly (3-sulphopropyl methacrylate) brushes Surface and Interface Analysis 42:855-858

Sadanand V, Tian H, Rajulu AV, Satyanarayana B (2017) Antibacterial cotton fabric with in situ generated silver nanoparticles by one-step hydrothermal method International Journal of Polymer Analysis and Characterization 22:275-279 doi:10.1080/1023666X.2017.1287828

Sambale F, Wagner S, Stahl F, Khaydarov RR, Scheper T, Bahnemann D (2015) Investigations of the Toxic Effect of Silver Nanoparticles on Mammalian Cell Lines Journal of Nanomaterials 2015:136765 doi:10.1155/2015/136765

Sankar R, Karthik A, Prabu A, Karthik S, Shivashangari KS, Ravikumar V (2013) Origanum vulgare mediated biosynthesis of silver nanoparticles for its antibacterial and anticancer activity Colloids and surfaces B, Biointerfaces 108:80-84 doi:10.1016/j.colsurfb.2013.02.033

Singh R, Wagh P, Wadhwani S, Gaidhani S, Kumbhar A, Bellare J, Chopade BA (2013) Synthesis, optimization, and characterization of silver nanoparticles from Acinetobacter calcoaceticus and their enhanced antibacterial activity when combined with antibiotics Int J Nanomedicine 8:4277-4290 doi:10.2147/IJN.S48913

Sivakumar P, Lee M, Kim YS, Shim MS (2018) Photo-triggered antibacterial and anticancer activities of zinc oxide nanoparticles J Mater Chem B 6:4852-4871 doi:10.1039/c8tb00948a

Somu P, Paul S (2019) Supramolecular nanoassembly of lysozyme and α-lactalbumin (apo α-LA) exhibits selective cytotoxicity and enhanced bioavailability of curcumin to cancer cells Colloids and surfaces B, Biointerfaces 178:297-306 doi:10.1016/j.colsurfb.2019.03.016

Song J, Kang H, Lee C, Hwang SH, Jang J (2012) Aqueous Synthesis of Silver Nanoparticle Embedded Cationic Polymer Nanofibers and Their Antibacterial Activity ACS Applied Materials & Interfaces 4:460-465 doi:10.1021/am201563t

Sotiriou GA (2013) Biomedical applications of multifunctional plasmonic nanoparticles WIREs Nanomedicine and Nanobiotechnology 5:19-30 doi:https://doi.org/10.1002/wnan.1190

Taylor WF, Moghadam SE, Moridi Farimani M, N. Ebrahimi S, Tabefam M, Jabbarzadeh E (2019) A multi-targeting natural compound with growth inhibitory and anti-angiogenic properties re-sensitizes chemotherapy resistant cancer PloS one 14:e0218125

Uddin KMA, Lokanathan AR, Liljeström A, Chen X, Rojas OJ, Laine J (2014) Silver nanoparticle synthesis mediated by carboxylated cellulose nanocrystals Green Materials 2:183-192

Vijayakumar S, Malaikozhundan B, Saravanakumar K, Durán-Lara EF, Wang M-H, Vaseeharan B (2019) Garlic clove extract assisted silver nanoparticle–Antibacterial, antibiofilm, antihelminthic, anti-inflammatory, anticancer and ecotoxicity assessment Journal of Photochemistry and Photobiology B: Biology 198:111558

Vijayan R, Joseph S, Mathew B (2019) Anticancer, antimicrobial, antioxidant, and catalytic activities of green-synthesized silver and gold nanoparticles using Bauhinia purpurea leaf extract Bioprocess Biosyst Eng 42:305-319 doi:10.1007/s00449-018-2035-8

Wu C-N, Fuh S-C, Lin S-P, Lin Y-Y, Chen H-Y, Liu J-M, Cheng K-C (2018) TEMPO-Oxidized Bacterial Cellulose Pellicle with Silver Nanoparticles for Wound Dressing Biomacromolecules 19:544-554 doi:10.1021/acs.biomac.7b01660

Wu J, Zhao N, Zhang X, Xu J (2012) Cellulose/silver nanoparticles composite microspheres: eco-friendly synthesis and catalytic application Cellulose 19:1239-1249 doi:10.1007/s10570-012-9731-3

Wu J et al. (2014) In situ synthesis of silver-nanoparticles/bacterial cellulose composites for slow-released antimicrobial wound dressing Carbohydrate polymers 102:762-771

Yi H et al. (2019) Ultra-Adaptable and Wearable Photonic Skin Based on a Shape-Memory, Responsive Cellulose Derivative Advanced Functional Materials 29:1902720

Yun YH, Lee BK, Park K (2015) Controlled Drug Delivery: Historical perspective for the next generation Journal of controlled release : official journal of the Controlled Release Society 219:2-7 doi:10.1016/j.jconrel.2015.10.005

Zhang X, Sun H, Tan S, Gao J, Fu Y, Liu Z (2019) Hydrothermal synthesis of Ag nanoparticles on the nanocellulose and their antibacterial study Inorganic Chemistry Communications 100:44-50

Zhang XF, Liu ZG, Shen W, Gurunathan S (2016) Silver Nanoparticles: Synthesis, Characterization, Properties, Applications, and Therapeutic Approaches International journal of molecular sciences 17 doi:10.3390/ijms17091534

Zhao R et al. (2017) Stable Nanocomposite Based on PEGylated and Silver Nanoparticles Loaded Graphene Oxide for Long-Term Antibacterial Activity ACS Applied Materials & Interfaces 9:15328-15341 doi:10.1021/acsami.7b03987

Figures

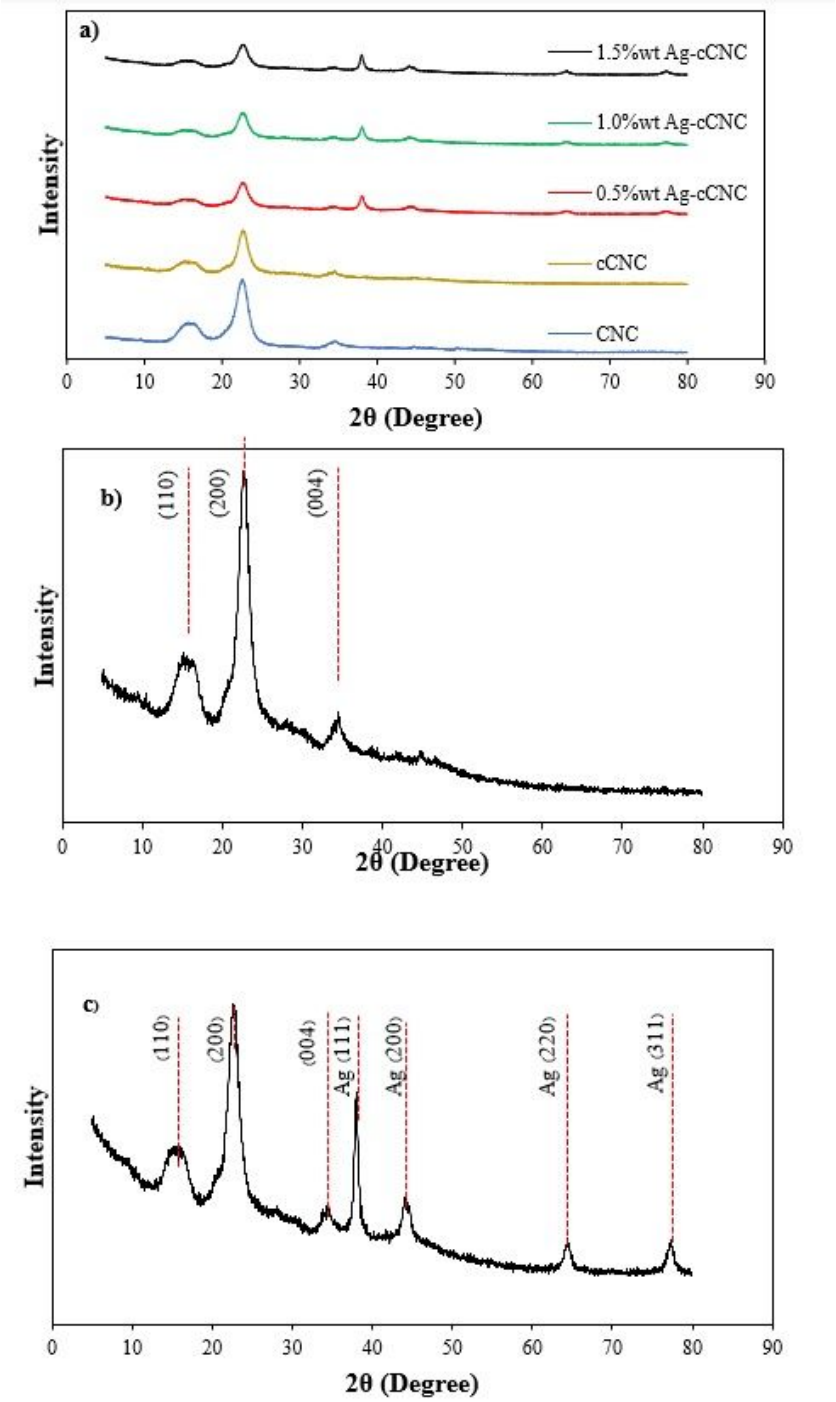

Figure 1

XRD pattern of CNC, cCNC and various Ag-cCNC concentrations (a), cCNC (b) and 1.5 wt%Ag-cCNC (c).

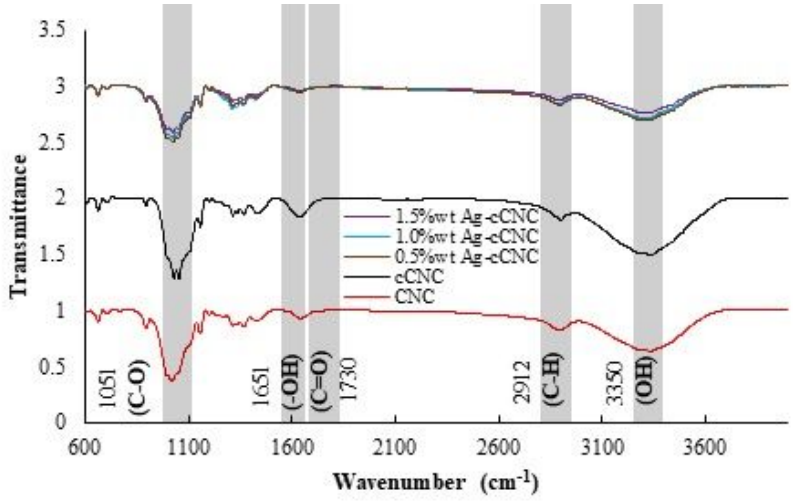

Figure 2

FTIR spectra of CNC, cCNC and various Ag-cCNC concentrations.

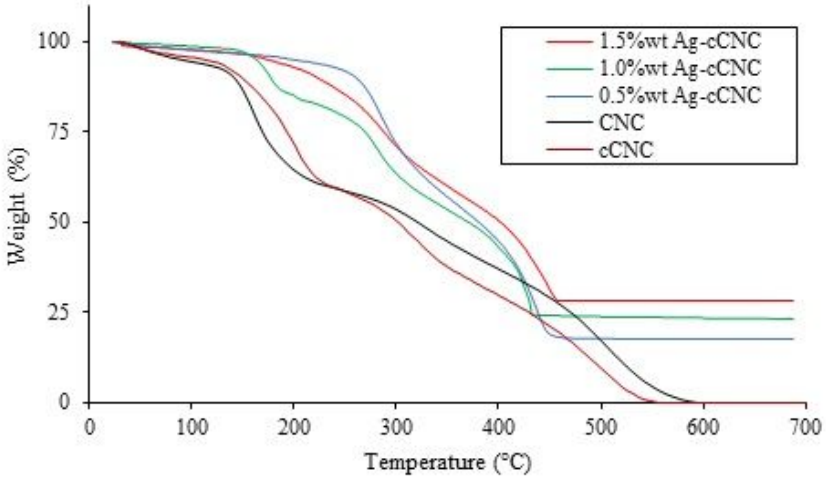

Figure 3

TGA curves of CNC, cCNC and various Ag-cCNC concentrations

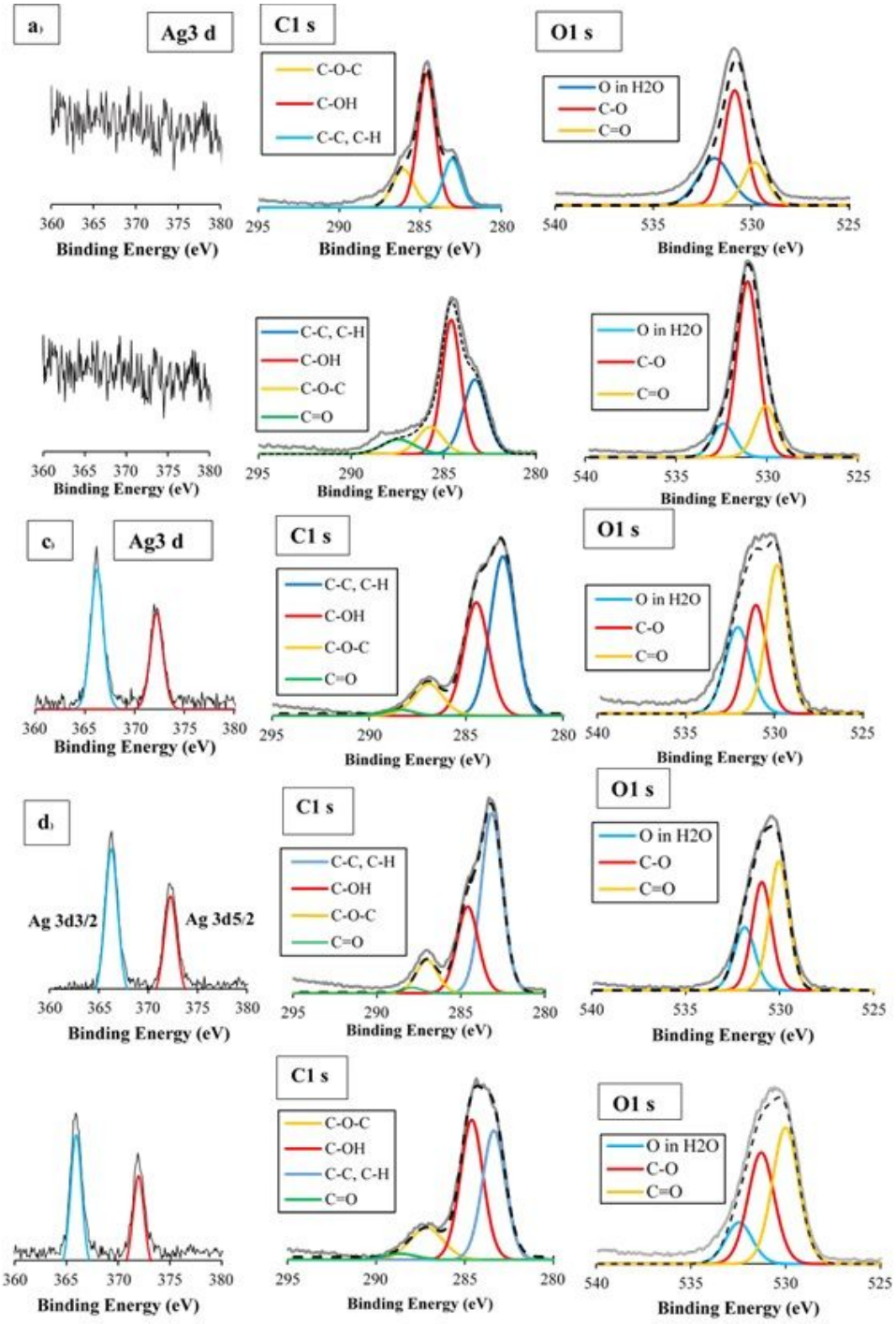

Figure 4

XPS spectra of CNC (a), cCNC (b), 0.5wt% Ag-cCNC (c), 1.0wt% Ag-cCNC (d), and 1.5wt% Ag-cCNC (e)

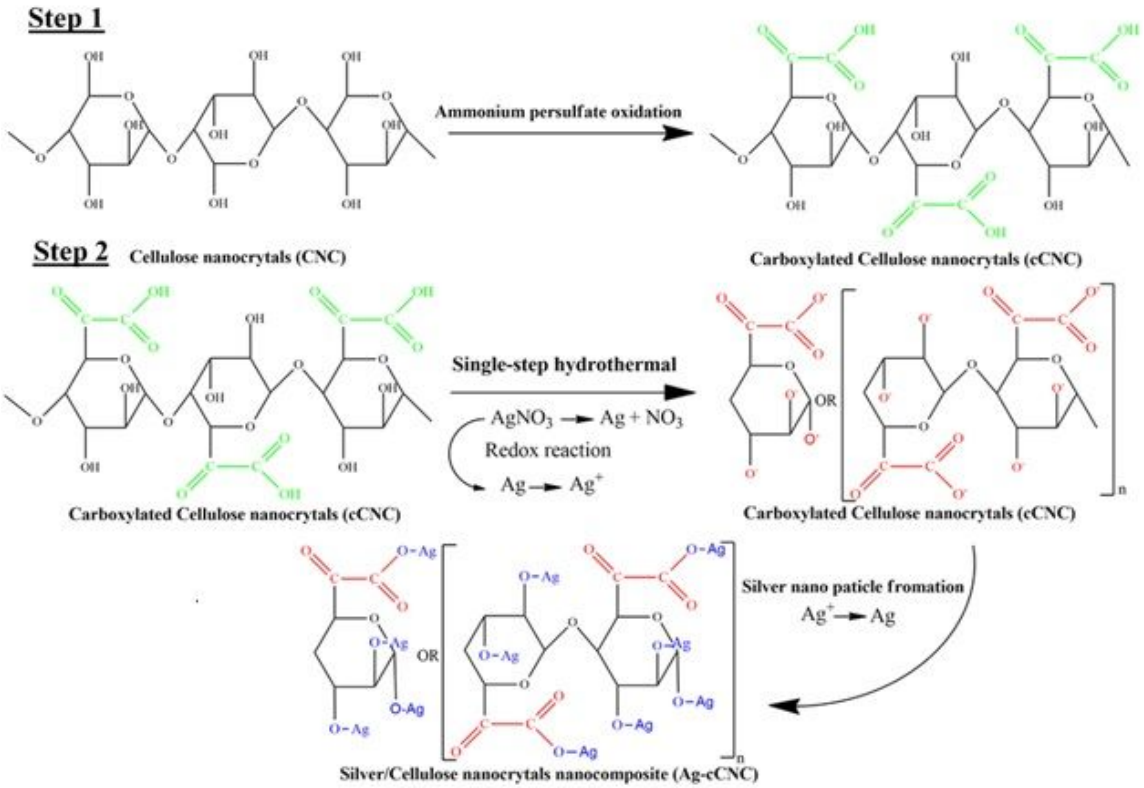

Figure 5

possibility mechanism of Ag-cCNC synthesis by hydrothermal reaction modified from Li, J., et al. (2019) work's (Li et al. 2019).

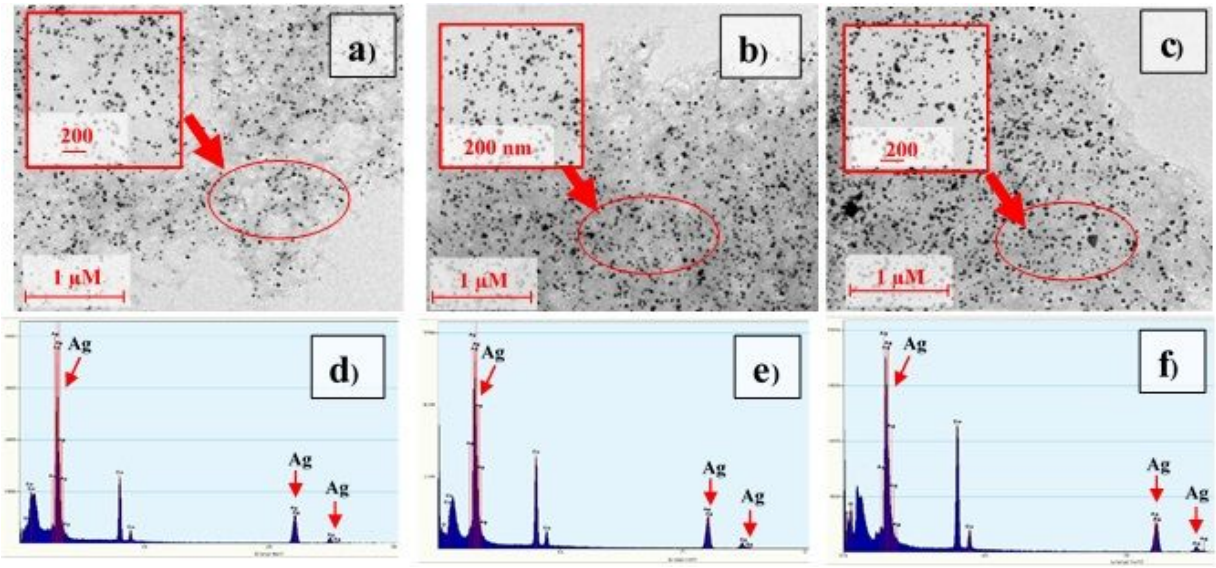

Figure 6

TEM image of (a)0.5, (b)1.0, and (c) 1.5wt% Ag-cCNC and EDX spectra (energy 0 – 30 keV) of (d) 0.5,(e) 1.0, and (f) 1.5wt% Ag-cCNC.

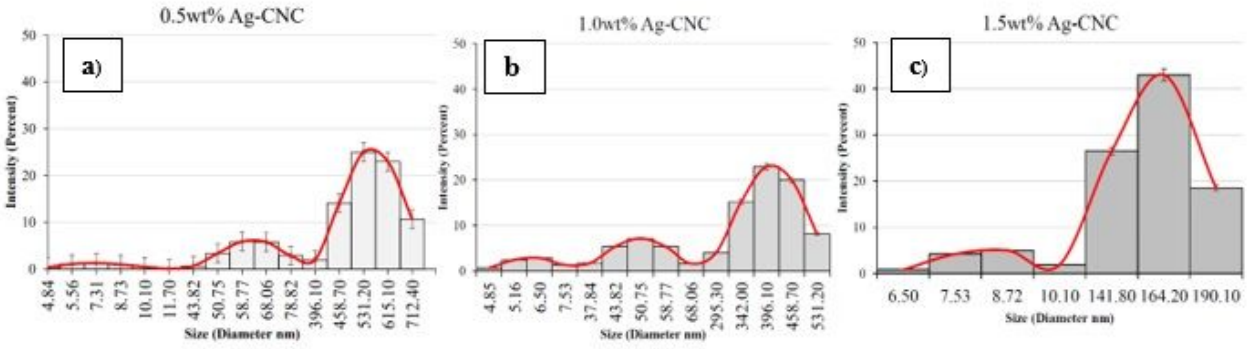

Figure 7

Size distribution of (a) 0.5wt% Ag-cCNC, (b)1.0wt% Ag-cCNC and (c) 1.5wt% Ag-cCNC.

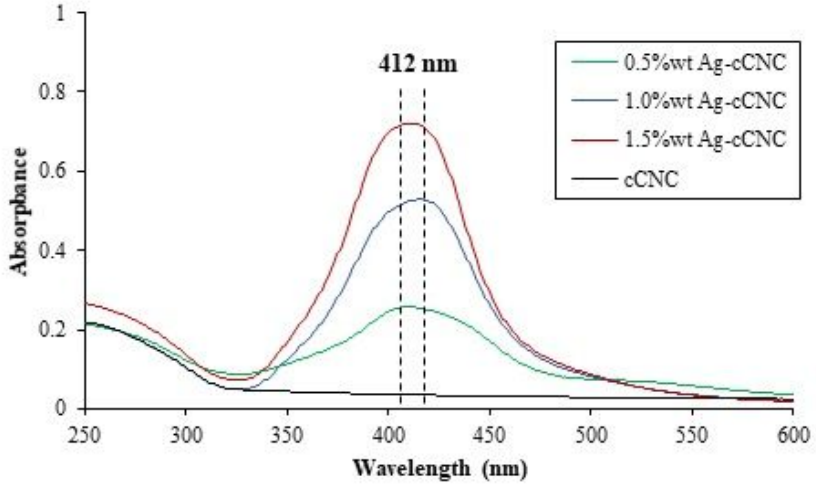

Figure 8

The spectra of Ag nanoparticle in Ag-cCNC composite at various concentrations by UV-VIS spectrophotometer analysis.

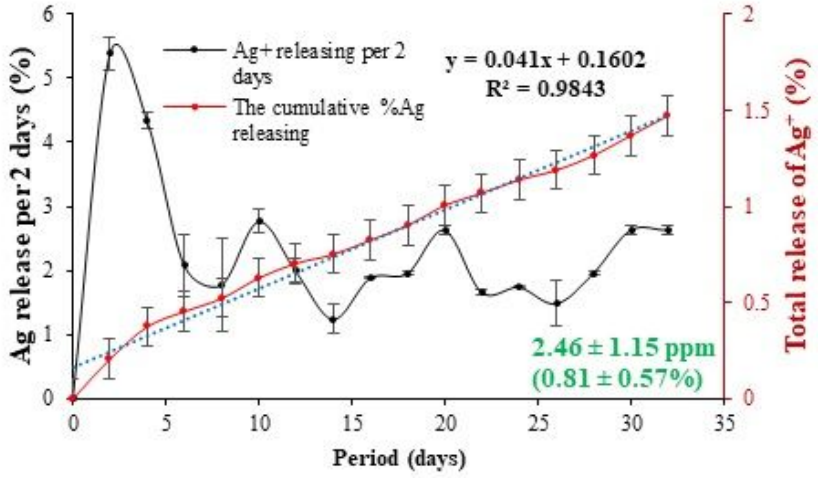

Figure 9

Ag+ release rate and total release of Ag+ behaviour of 1.5wt% Ag-cCNC in DI water at 37 °C for 32 days.

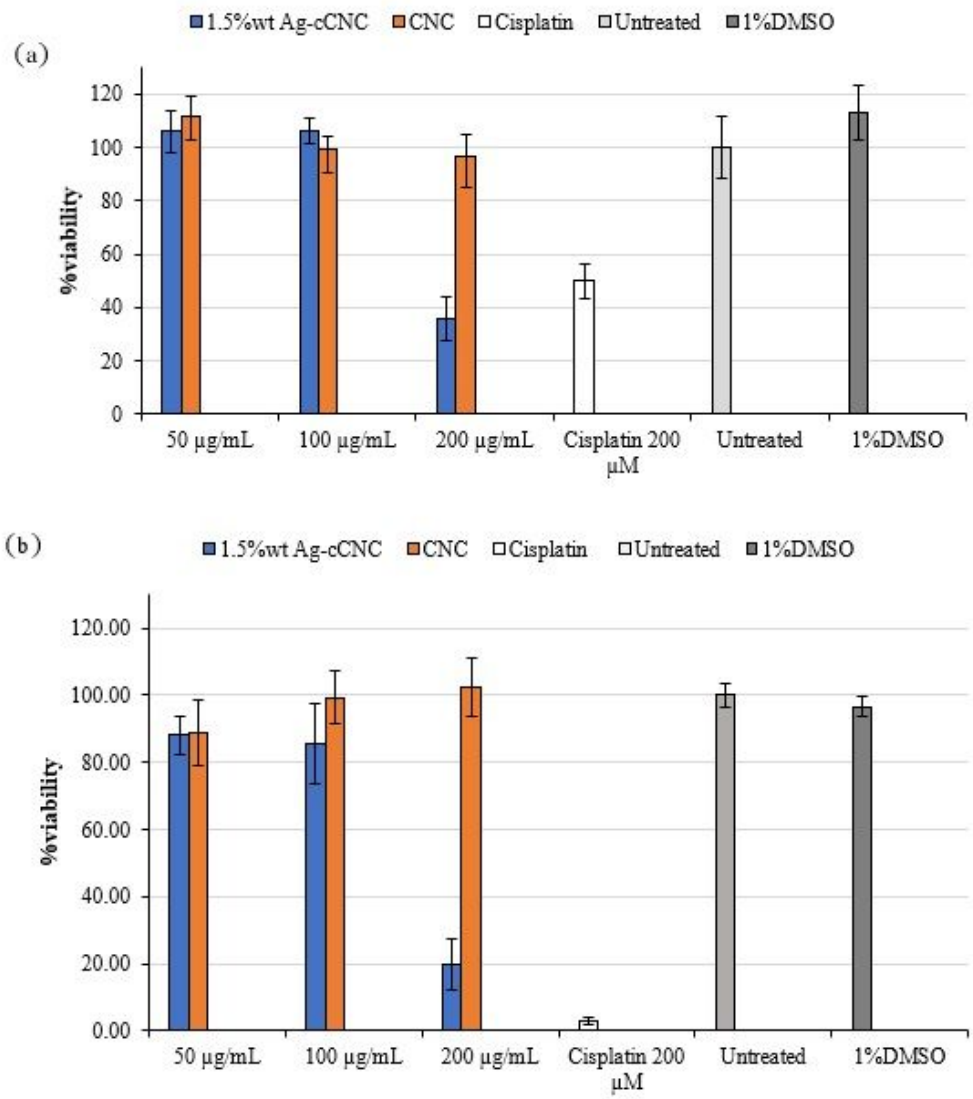

Figure 10

Percentage of the viability of HCT116 cancer cell line (a) and SK-MEL-2cancer cell line (b) against various cNC and 1.5wt% Ag-cCNC doses, Cisplatin, 1%DMSO and Control (untreated cell)

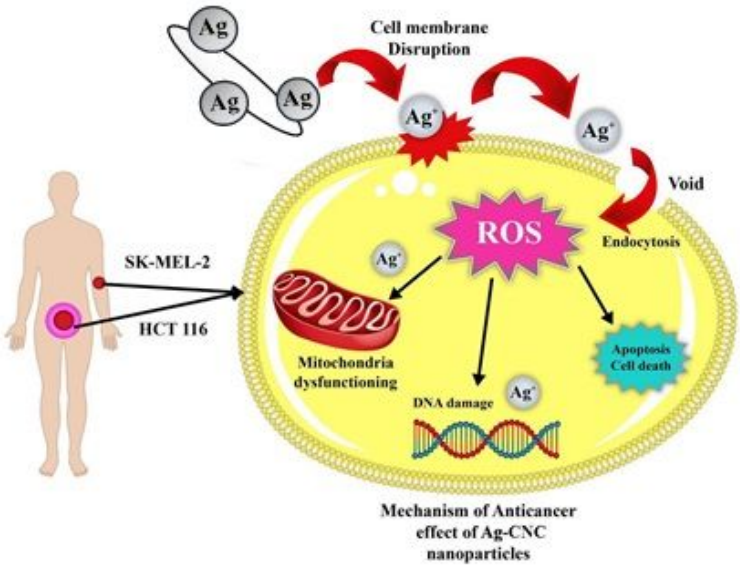

Figure 11

Graphical representation of anticancer mechanisms of Ag-cCNC

Supplementary Files

This is a list of supplementary files associated with this preprint. Click to download.

- Supplementarydata15032021.docx
- GraphicalAbstract.jpg